Resistive switching effect and traps in partially fluorinated graphene films

2016 J. Phys. D: Appl. Phys. 49 095303

(http://iopscience.iop.org/0022-3727/49/9/095303)

IOP Publishing Journal of Physics D: Applied Physics
J. Phys. D: Appl. Phys. **49** (2016) 095303 (9pp) doi:10.1088/0022-3727/49/9/095303

Resistive switching effect and traps in partially fluorinated graphene films

Irina I Kurkina[1], Irina V Antonova[2,3], Nadezhda A Nebogatikova[2], Albert N Kapitonov[1] and Svetlana A Smagulova[1]

[1] Ammosov North-Eastern Federal University, 677000, Belinsky Street 58, Yakutsk, Russia
[2] Rzhanov Institute of Semiconductor Physics SB RAS, 630090, Lavrentiev Avenue 13, Novosibirsk, Russia
[3] Novosibirsk State University, 630090, Pirogov Street 6, Novosibirsk, Russia

E-mail: antonova@isp.nsc.ru

Received 18 September 2015, revised 7 December 2015
Accepted for publication 8 December 2015
Published 2 February 2016

Abstract

A reversible resistive switching effect is detected in films created from the suspension of partially fluorinated graphene (more specifically, small graphene or few-layer graphene quantum dots in a fluorographene matrix), which makes them promising for resistive memory applications. This paper is focused on the investigation and comparison of the traps and transport in such films in both the low- and high-resistance state. The appearing set of traps for holes and electrons in the band gap of fluorinated graphene is revealed in the films at the low-resistance state, and their parameters (activation energy and trap density) are defined using charge spectroscopy. The minimum relaxation time of nonequilibrium carriers from different traps is found to be about 700 ns, and the energy level position of corresponding traps from the conduction band of a silicon substrate equals 0.08 eV. It has also been demonstrated that the carrier transport in the low-resistance state is determined by the same traps, and they form conductive channels in the film. Transport and non-equilibrium recharging processes in the state of high resistance are found to occur above all by means of carrier tunneling through the potential barriers in the films.

Keywords: fluorinated graphene, resistive switching effect, localized traps, carrier transport

(Some figures may appear in colour only in the online journal)

1. Introduction

Distinctive changes have been taking place in data storage technology for several decades. The flash-memory advent can be called a revolutionary step in this area of development. Superfast chips, capable of storing a huge amount of information, shall be the next milestone [1]. In recent times, much effort has been invested in the creation of simple-to-manufacture and reliable elements of nonvolatile resistive memory, which is expected to become a serious competitor to traditional flash devices. When voltage is applied to the resistive memory element, the transition into the state with low resistance takes place. Indeed, the reverse transition is also possible, for example, by applying a voltage of different polarity (bipolar switching regime). Typically, resistive memory elements are based on thin films of metal oxides (TiO_2, Cr_2O_3, FeO_x, NiO, etc), high constant dielectrics (Al_2O_3, HfO_2, Gd_2O_3) and some other materials. Currently, the resistive memory approach is considered the most promising, as it allows us to obtain a significantly lower time of data overwriting (for instance, one microsecond for TaO_x [2] and even five nanoseconds for TiO_2 [3]). The lower the overwriting voltage (lower than 3 V), the longer the period of information storage, and the higher the number of rewriting cycles [1–3]. But, up to now, there has been no industrial production of non-volatile resistive memory elements. One of the problems of metal oxide materials is the relatively high temperature for their fabrication. Moreover, the obstacles to industrial production of oxide-based resistance switching memories are unclear resistive switching mechanisms and wide programming parameter distributions.

Lately, some effort has been made to create the resistive memory from graphene oxide [4–6] or MoS_2 graphene oxide

composite [7]. Recent interest in the graphene-based materials results from its possible use in the manufacture of flexible resistive memory elements [8]. Partially fluorinated graphene (FG) turned out to show the resistive switching effect as well (the first observation of the resistive effect for FG is given in the present study). More precisely, partially fluorinated graphene films consist of small graphene or few-layer graphene quantum dots in a fluorinated graphene matrix [9]. Graphene oxide also consists of graphene areas and a chemically modified part of the material. So, in both cases, we have two-phase systems and both parts contribute to the layer properties. The high carrier mobility in graphene (up to 2×10^5 cm^2 Vs^{-1} at room temperature) and the short relaxation time of the nonequilibrium charge (~10^{-13} s) are expected to provide a high speed of resistance switching in memory device structures [10, 11]. This statement is based, for instance, on the results of a charge deep-level transient spectroscopy (*Q*-DLTS) study of carrier capture/emission from graphene quantum dots in a fluorinated matrix that demonstrated the possibility of a strong decrease (at least on ~four orders of magnitude) in the carrier transport time in multilayer films of fluorinated graphene and/or under daylight illumination [12, 13]. For fluorinated graphene, the overwriting time is still unknown. In the case of the films created from graphene suspension, the switching time is determined, first of all, by the short relaxation time of the nonequilibrium charge in graphene with the reduction due to structural imperfections. For graphene or graphene oxide structures this time is generally lower than 1 μs [14] (overwriting time ~1 μs for a GO composite [15], the fast switching speed down to 500 ns for a planar graphene/SiO_2 nanogap structure [16], the switching speed of <5 ns for GO noncovalently functionalized by thionine [17], etc).

Different models of resistance switching are suggested for graphene oxide (migration of electrode metal ions, or oxygen-related functional groups, oxygen vacancies [3, 14]), but the physics of resistive switching has not been fully understood [1]. Moreover, the stability of graphene oxide is known to be relatively low. Insignificant heating or electrical current flowing can significantly change the resistance of graphene oxide films. At the same time, fluorinated graphene is known to have much higher stability and reproducibility of properties. Defluorination of fluorographene occurs at 400–450 °C [18], whereas the recovery of graphene oxide starts at 100–200 °C [19].

In addition to the first observation of the resistive effect for partially fluorinated graphene, in the present study we investigate traps and carrier transport in the films of partially fluorinated graphene in a low-resistance state and compare them to the traps and carrier transport in the same films in a high-resistance state. In the low-resistance state, films formed from fluorinated graphene suspension demonstrate the presence of conductive channels on the traps for holes and electrons in the FG band gap, which parameters (energies and densities) were identified using the *Q*-DLTS. The times of the nonequilibrium charge relaxation from different traps have also been determined and compared. The traps with the energy level position 0.08 eV from the conduction band of the silicon substrate are found to have the minimum relaxation time (about 700 ns). These traps were demonstrated to form the conductive channels in the low-resistance state of partially fluorinated graphene films.

2. Experimental section

2.1. Sample preparation

The initial material for the creation of fluorinated graphene films is a graphene suspension. The direct preparation of graphene dispersions is possible in polar and nonpolar organic solvents [20, 21]. In our study, the suspension is obtained by natural graphite grinding, dispersion in dimethylformamide (DMF) with a graphite flake weight concentration of 0.2 mg ml^{-1}. Then, the composite is subjected to ultrasonic machining for the graphite flakes to split off. DMF provides a high concentration of graphene sheets and suspension stability [22, 23]. The graphene suspension is fluorinated with the use of a 3% aqueous solution of hydrofluoric acid [24, 25]. After a proper fluorination time, centrifugation at high rate with the subsequent replacement of the HF solution in the water allows us to obtain a suspension with small and thin graphene flakes in water. Silicon plates with p- and n-type conductivity (carrier concentration ~5×10^{15} cm^{-3}) are used as substrates for the films from graphene suspension. In this study, we opt for silicon substrates (not metal electrodes) because a semiconductor provides an injection of both types of carriers into the tested film under different applied voltage polarities that enables the observation of the whole spectrum of traps in the film. Films were prepared by pouring droplets of the suspension on the silicon substrate, drying, rinsing in deionized water to remove the residual hydrofluoric acid and the organic component of the suspension, and drying for water removal for the second time. It should be noted that fluorination of the suspension changes the wettability of silicon substrates with respect to suspension droplets: the fluorinated suspension easily spreads over the substrate surface and forms a thin continuous film.

2.2. Methods

To obtain data on the fluorinated graphene film structure the scanning electron microscope (SEM) JEOLJSM-7800F with the energy of primary electrons equal to 2 keV is used. For taking atomic force microscope (AFM) images of the film and substrate surfaces and for determining the film thicknesses, a Solver PRO NT-MDT scanning microscope is used. Measurements are performed both in contact and semi-contact mode. Raman spectra are measured at room temperature; the excitation wavelength is 532 nm (2.33 eV). Measurements are carried out at the Integra Spectra (NT-MDT) facility. In order to avoid sample heating with laser-emitted radiation, the laser beam power is decreased to 2–3 mW. The spectra are recorded using the NT MDT Nanolaboratory INTEGRA Spectra spectrometer. Electrical measurements are carried out with the automated system ASEC-03. Gold contacts with the area of 0.49 mm^2 are deposited using sputtering on fluorinated graphene films for measurements in both configurations.

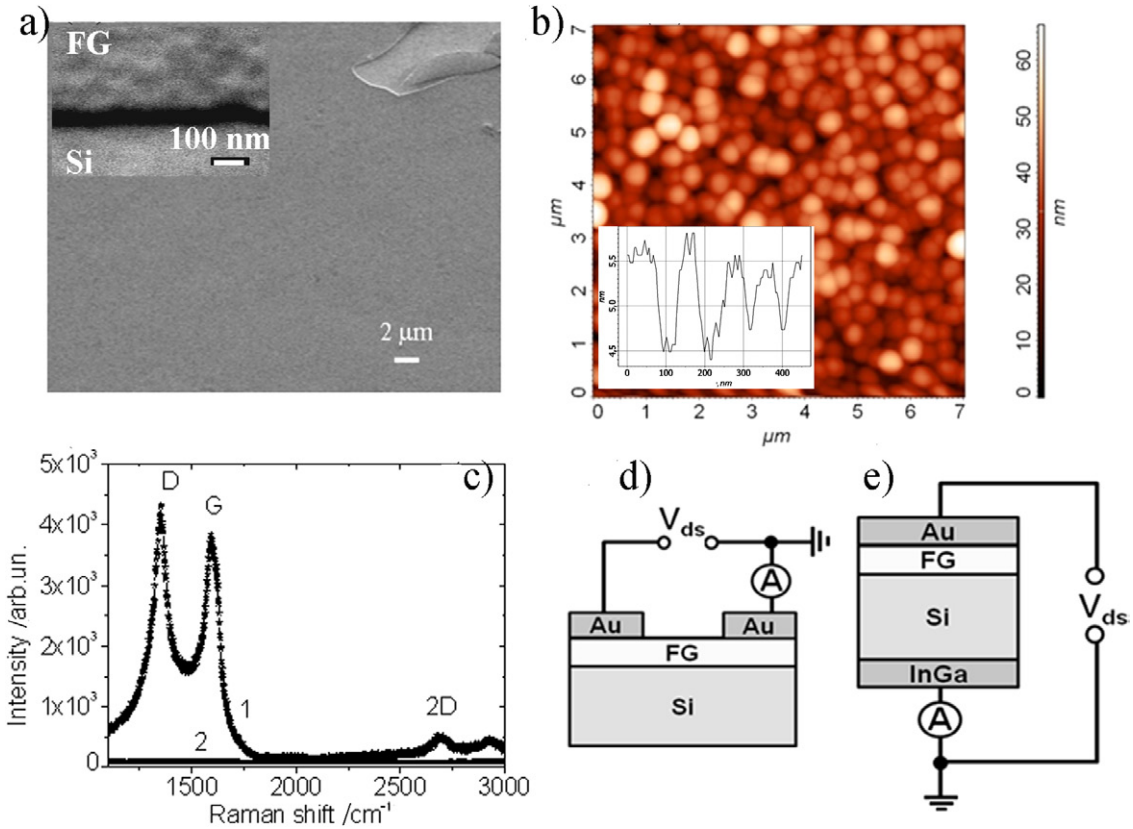

Figure 1. (a) Surface image of partially fluorinated graphene film, obtained by a scanning electron microscope. The smooth homogeneous surface of the film has roughness of about 10 nm. The surface roughness decreases with an increase of fluorination degree up to 2 nm. The film defect in the upper right corner of the image demonstrates the presence of the film on the silicon surface. The insert presents the image of the film obtained under 45°. The estimated film thickness is equal to ~100 nm. (b) Image of the FG surface, obtained by an atomic force microscope. The insert gives the profiles for flakes with thickness ~from 0.4 to 1.1 nm. (c) The Raman spectra of the film from unfluorinated pristine suspension (1) and the film from fluorinated suspension (2). (d, e) The lateral and vertical configurations, respectively, are schemes used for electrical measurements.

Ohmic contact from InGa paste is applied to the silicon substrate from the bottom in the case of measurements in the vertical configuration.

Q-DLTS measurements are performed using an ASEC-03 DLTS spectrometer. In the *Q*-DLTS measurements, filling voltage pulses V_{fp} provide for graphene island charging; the emission of charges from the graphene islands is subsequently measured. Such measurements are performed by varying the rate window τ_m, while keeping the temperature unchanged. Here, the rate window is determined as

$$\tau_m = \frac{(t_2 - t_1)}{\ln\left(\frac{t_2}{t_1}\right)},$$

where t_1 and t_2 are the times at which the *Q*-DLTS signal due to the relaxation of the dielectric-trapped charge $\Delta Q = Q(t_2) - Q(t_1)$ is observed at the end of a filling pulse. The amplitude of filling pulses V_{fp} was 2–4 V, and the width of the pulses can be varied from 30 μs to 2 s. The constant voltage applied to the sample after the end of the filling pulse has to provide the conditions for the carrier emission from the traps. In the present study, we have used the constant voltage up to ±4 V in the case of lateral *Q*-DLTS measurements and $U = 0$–1 V in the case of vertical *Q*-DLTS measurements. In both cases, the currents are limited by values of 10^{-8}–10^{-6} A. The concentration of the trapping centers can be obtained from the *Q*-DLTS peak amplitude. The time of the carrier emission from the traps is determined from the maximum position of the corresponding peak τ_m. Thus, the analysis of measured *Q*-DLTS spectra allows for the estimation of the following parameters of localized states in our samples: number of traps, the nonequilibrium carrier emission (relaxation) time, the activation energy, and the density of every trap. The time of the hole/electron emission τ_m from the traps in a bulk semiconductor material is [26]

$$\tau_m^{-1} = \sigma \nu_F N_C \exp\left(\frac{-E_a}{kT}\right) \quad (1)$$

where σ is the carrier capture cross-section, T is the temperature, E_a is the activation energy, $N_C = 4\frac{E}{2\pi\hbar^2 v_F^2} = 4\frac{\sqrt{n_s}}{2\sqrt{\pi}}$ is the density of states in the conduction band of graphene [27], n_s is the charge carrier density, $\hbar$ is the reduced Planck constant, k is the Boltzmann constant, and v_F is the Fermi velocity in the vicinity of the K points of the graphene band structure ($v_F = 10^6$ m s^{-1}). Using formula (1), activation energies E_a can be derived from the Arrhenius curves, plotted in coordinates $\ln(\tau_m^{-1})$ versus $1/T$. The concentration of the trapping centers can be obtained from the *Q*-DLTS peak

amplitude. The time of the carrier emission from the traps is determined from the maximum position of the corresponding peak τ_m. The density of traps N_t is proportional to the maximum differential charge $\Delta Q_{\max}$ of the corresponding Q-DLTS peak, for instance, at room temperature. $N_t = 4\Delta Q_{\max}/qA$, where q is the charge of the electron, and A is the area of the contact.

3. Experimental results

To obtain data on the structure of fluorinated graphene films the SEM and AFM are used. Figures 1(a) and (b) show images of the fluorinated graphene surface, obtained by SEM and AFM, respectively. The thickness of the produced films is determined using SEM and equals several tens of nanometers (50–100 nm). As may be inferred from the AFM data, the fluorinated graphene film consists of flakes with the size of 200–400 nm and thickness of 1–4 ml (0.4–1.5 nm); in addition, there were flakes of smaller sizes (20–30 nm) (see insert in figure 1(b) and for details [9]).

Figure 1(c) shows typical spectra of Raman scattering for the film, formed from pristine (non-fluorinated) suspension, as well as for the film from the fluorinated suspension. The Raman spectrum for the film of pristine graphene suspension has three main lines. Line G is about 1582 cm^{-1} and is associated with the doubly degenerate phonon modes in the center of the Brillouin zone (point D) [28]; it is caused by vibrations of carbon atoms in the plane of the graphene layer. 2D and D lines are derived from the second-order process with two planar transverse phonons near K point for the 2D line, as well as one phonon or one defect in the case of the D line. Line D is caused by vibrations of carbon atoms of dangling bonds at the edges of the graphene flakes [29]. When graphene suspension is treated in the aqueous solution of hydrofluoric acid, the graphene changes electronic structure and the band gap appears. With an increase in time of the graphene suspension fluorinated treatment, the intensity of all peaks in the Raman spectrum first begins to decrease, and then, when the value of the band-gap energy reaches or overcomes the value of exciting radiation (2.33 eV), the peaks vanish (figure 1(c) Line 2) [9].

Electrical measurements are carried out in two configurations: lateral and vertical, schematically represented in figures 1(d) and (e), respectively. Contacts are prepared by means of gold evaporation or using argentum alloy. InGa alloy is used for the contact with the Si substrate.

Figure 2 shows current–voltage characteristics for vertical Au/FG/Si/InGa structures and lateral Au/FG/Au structures, measured at two voltage sweeps. It can be seen that the transition to the lower resistance of the layer occurs at a voltage of about −1.5 V in the vertical configuration and at about −4 V in the lateral one. The reverse transition occurs by changing the polarity of the applied voltage. Repeated measurements prove the repeatability of such switching. We have verified the repeatability of resistivity switching at least 120 times. After these cycles, the voltage of the resistance switching is increased from −1.5 to 1.9 V. The variation of temperature measurements from 80 to 350 K shows that these transitions may be observed in the entire studied temperature range.

Daylight illumination is very important for carrier transport in fluorinated films (see figure 2(c)). More pronounced effects are observed for the current at positive voltages. The reset loops observed in the case of dark conditions degrade under daylight illumination. The reason for this effect is connected with a strong decrease in the time of non-equilibrium carrier relaxation directly observed in similar structures [13]. The resistive switching effect, like that given in figure 2, had been observed for all structures with a certain fluorination degree (~50 structures). For a lower fluorination degree, the relation of resistances decreased, and for a higher fluorination degree the films became insulated.

According to previous studies of the FG films [9], the dielectric constant of this material is 3.2—1.1 depending on the fluorination degree, and the electric field strength, sustained by the film, is 1.2×10^6 V cm^{-1}. Capacitance–voltage measurements, performed on the films in the high-resistance state, show that the fixed charge in the films and the density of states at the FG/Si interface are low (~5×10^{10} cm^{-2}).

The study of current–voltage characteristics shows that long-term application of the electric field with the strength exceeding 1.2×10^6 V cm^{-1} (>6 V for the film with 50 nm thickness) to the film, leads to the high-conductivity state ceasing to be reversible. Using the mentioned treatment, we managed to study the distinctive features of the state of low resistivity. Annealing at temperatures of 130–150 °C for 10 min allowed for the film switching to the high-resistance state. After such annealing the reversible resistivity switching was observed again.

Figure 3 demonstrates temperature dependences of the current through the films with a thickness of 50 and 100 nm at two electric-field intensities. Two factors are important for further discussions. For a relatively low electric-field intensity (curve 1, high-resistance state), at the temperature range from 250 to 330 K, the current is described with equation $I = I_0 \exp(-E/kT)$, where E is the activation energy of the current flow through the film, and k is the Boltzmann constant. The obtained value of E is 0.48 eV for 100 nm films. For relatively high electric-field intensity (curve 2, low-resistance state), the activation energy E for both films is 0.09 eV at the temperature range from 150–170 to 330 K. At the lower temperatures the current is again near to the constant. It is particularly clearly observed for the film with 50 nm thickness. The activationless current flow through the film is, most likely, associated with carrier migration (tunneling) through the traps in the FG band gap or graphene inclusions. An increase in current value in the low-resistance state compared to the high-resistance state unequivocally asserts the introduction of new traps under high voltage.

The Q-DLTS was used to study the traps in the films from the partially fluorinated suspension both in the states of low and high resistance. Let us start with the Q-DLTS study of films in the low-resistance state. In the case of p-Si substrate, the peak associated with the major carriers in the substrate (holes) was detected in the spectra. Figure 4(a) presents Q-DLTS spectra for one of the samples and relatively high temperatures (200–330 K), and figure 4(c) shows the corresponding Arrhenius dependencies (group of lines with the same

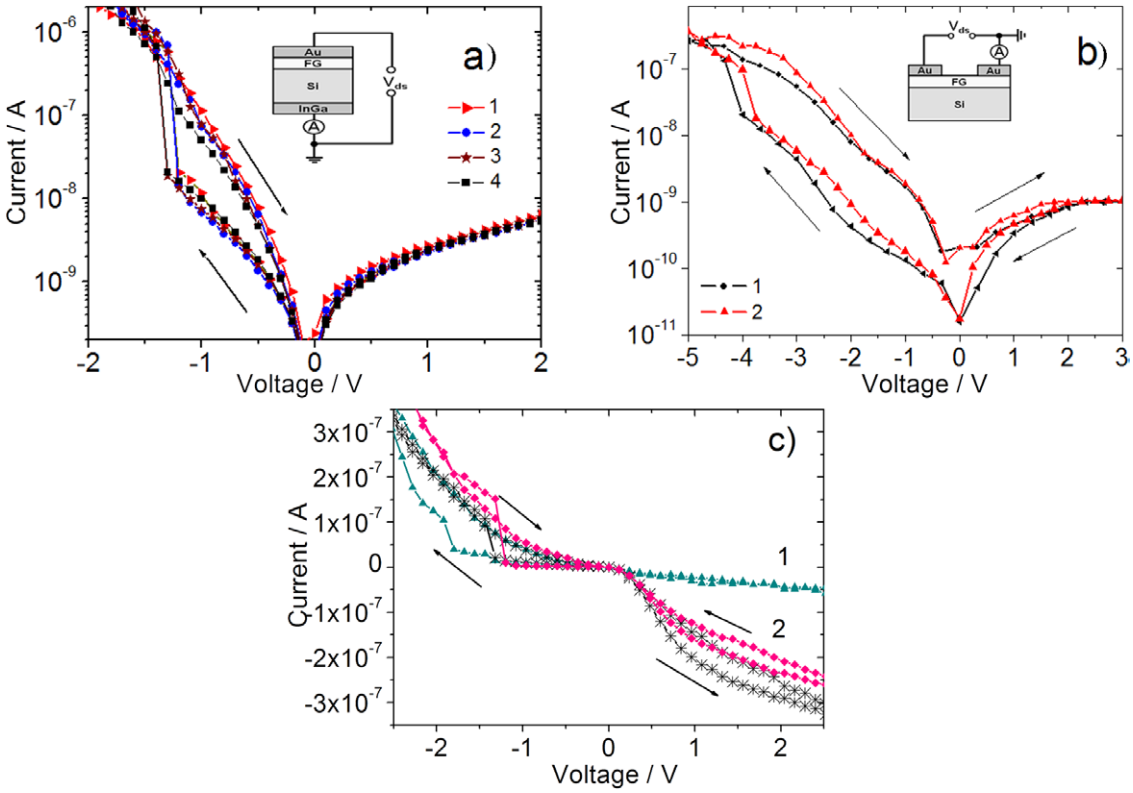

Figure 2. Current–voltage characteristics measured at daylight conditions of (a) vertical Au/FG/Si/InGa structures and (b) lateral Au/FG/Au structures (contact size was 0.5 mm, and period between contacts was 1.5 mm) measured several times at two voltage sweeps at the temperature of 300 K. (c) Vertical Au/FG/Si/InGa structures measured in daylight (1) and dark (2) conditions. Fluorinated graphene film has a thickness of 80 nm. The diagram of the used measurements configuration is shown on the insert.

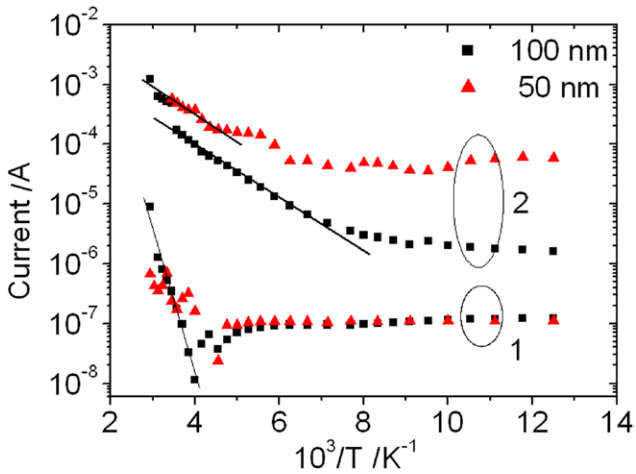

Figure 3. Temperature dependences of the current through the fluorinated graphene film on p-Si substrate at the electric field intensity of 5×10^5 V cm^{-1} (1) and 2.5×10^6 V cm^{-1} (2) measured in vertical configuration. Lines correspond to the activation energy 0.48 eV (1) and 0.09 eV (2).

slope and the activation energy, which is designated as E_1). At lower temperatures the observed peak in the *Q*-DLTS spectra stops shifting at temperature change. It corresponds to the non-activated emission of carriers from traps (points, specified as E_2 in figure 4(c)) in the band gap of the FG films, which agrees well with the temperature dependence of current in figure 3. Figure 6 shows the band diagrams of Au/FG/p-Si structures at zero voltage during the trap filling in FG with the carriers from the substrate, and during the carrier emission from the traps. Details of the band diagrams construction will be discussed below. Densities of the traps, activation energies and other parameters of the found traps are summarized in table 1. Similar centers (E_1–E_3) are observed in *Q*-DLTS spectra also in the case of measurements with lateral configuration of contacts on the film surface (see figure 1(d)). As film thickness is sufficiently small (50–150 nm), under applied voltage it is possible to fill the traps in the FG not only by electrons from the metal contacts, but also by the holes from the silicon substrate. At the use of temperatures below 120 K or at different polarity of the filling pulse voltage it is possible to observe the appearance of minor carrier peaks (figure 4(b)). Arrhenius curves determining the activation energy of the carrier emission from these traps are shown in figure 4(c) (the group of lines, designated as E_3).

In the case of n-Si substrate, it is also possible to observe one peak in *Q*-DLTS spectra, associated with the capture and emission of electrons from the traps in the FG band gap with energies E_4 and E_5 (see figure 4(a) and table 1).

The traps in the fluorinated films in the high resistivity state are also studied and compared using *Q*-DLTS. The parameters of these traps are given in table 1. Figure 5 presents the *Q*-DLTS spectra and Arrhenius plots for FG/p-Si structures. Only one type of activated energy $E_{01} = 0.5$ eV is detected, and other carrier relaxation channels turn out to be non-activated. For FG/n-Si structures only non-activated emission of

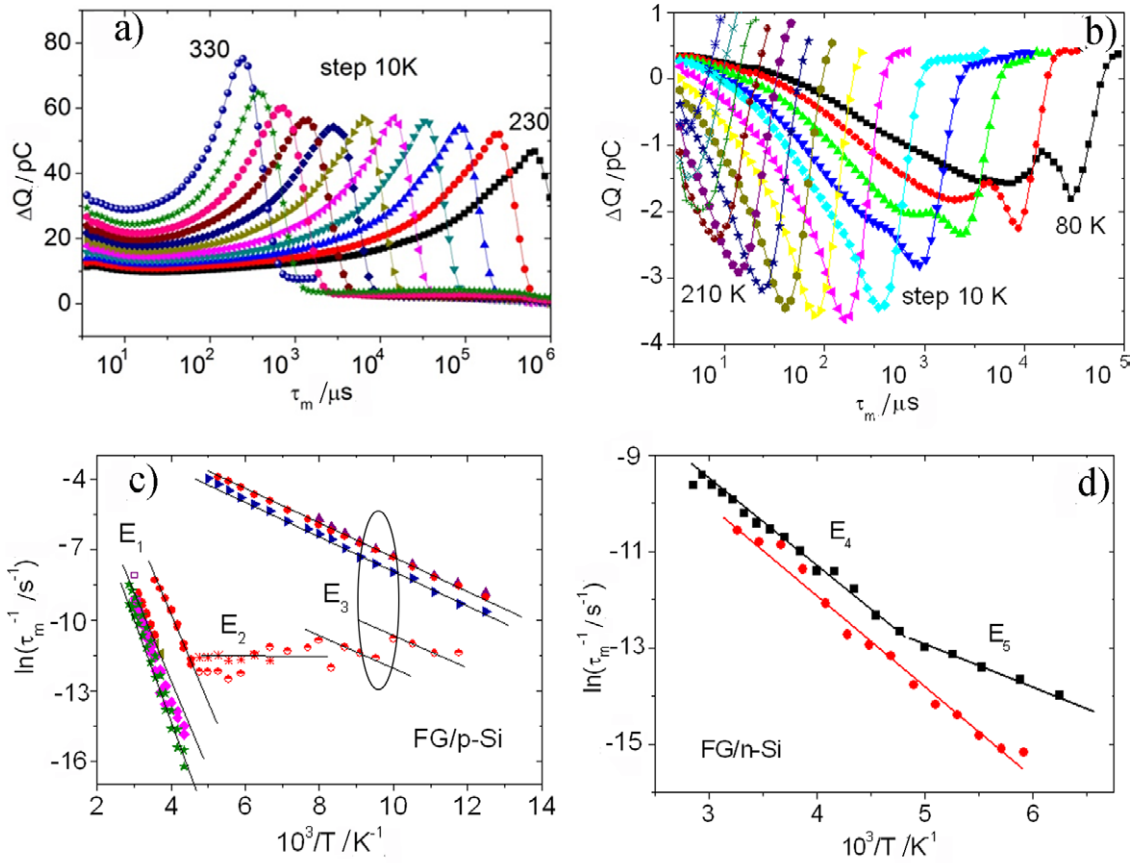

Figure 4. (a) Q-DLTS spectra for FG/p-Si structure in the low-resistance state, associated with the holes, which are consistent with the activation energy of the carriers E_1 and E_2 (the constant voltage is -4 V and the amplitude of the filling pulse is 5 V). (b) Q-DLTS spectra for the same structure, associated with the minor carriers (electrons), which correspond to the activation energy of the carrier E_3 (constant voltage is 2 V and the amplitude of the filling pulse is -3 V). (c) Arrhenius plots for FG/p-Si structures with activation energies $E_1 = 0.34$ eV, $E_2 = 0$ eV, $E_3 = 0.08$ eV; measurements are performed both in the lateral (one line in E_1 group and one line in E_3 group) and vertical configurations. Accuracy of energy determination is 0.02 eV. Different lines (points) correspond to measurements on different samples. (d) Arrhenius plots for FG/n-Si structures with activation energies $E_4 = 0.15$ eV, $E_2 = 0.12$ eV. Q-DLTS spectra correspond to vertical structures (figure 1(e)). Arrhenius plots include data for both vertical and lateral structures (figure 1(e)).

Table 1. Parameters of the traps, detected by the Q-DLTS method in the FG films on the p- and n-silicon substrate (activation energy E_i and densities N), temperatures of trap monitoring and time of nonequilibrium carrier emission from the traps at room temperature.

Structure	Activation energy E	Density N	Temperature	Emission time, 300 K
High-resistance state				
FG/p-Si	Hole traps			
	$E_{01} = 0.50$ eV	9.6×10^{12} cm^{-2}	350–280 K	10^{-3} s
	$E_{02} = 0.00$ eV	6.8×10^{12} cm^{-2}	270–150 K	10^{-2} s
	Electron traps			
	$E_{03} = 0.00$ eV	7.9×10^{12} cm^{-2}	350–150 K	0.3 s
FG/n-Si	Hole traps			
	$E_{04} = 0{,}00$ eV	6.5×10^{11} cm^{-2}	300–160 K	10^{-2} s
Low-resistance state				
FG/p-Si	Hole traps			
	$E_1 = 0.38$ eV	6×10^{10} cm^{-2}	320–280 K	10^{-4} s
	$E_2 = 0.00$ eV	3×10^{10} cm^{-2}	270–200 K	10^{-2} s
	Electron traps			
	$E_3 = 0.08$ eV	2×10^{10} cm^{-2}	210–80 K	$<10^{-6}$ s
FG/n-Si	Electron traps			
	$E_4 = 0.15$ eV	1.4×10^{12} cm^{-2}	350–200 K	10^{-4} s
	$E_5 = 0.12$ eV	1.4×10^{12} cm^{-2}	200–150 K	

Note: Accuracy of energy determination is 0.02 eV.

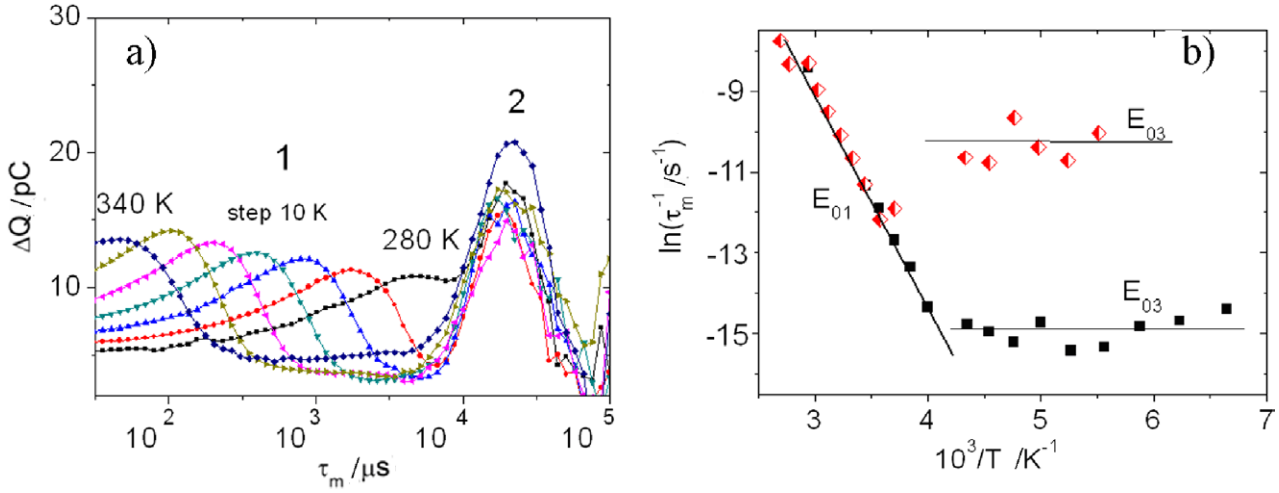

Figure 5. (a) Q-DLTS spectra for FG/p-Si structures in the high-resistance state, associated with holes consistent with the activation energy of the carriers E_{01} (1) and E_{03} (2); used voltages are $U = 1$ V, $\Delta U = -2$ V. (b) Arrhenius plots for studied structures. Different lines correspond to measurements on different contacts.

carrier is observed. Non-activated carrier emission processes with varying emission times, most likely, correspond to carrier tunneling through the barrier with different parameters (barrier height and/or thickness).

One of the most important parameters of the material for resistive memory is the time of switching from the high-resistance state to the low-resistance state. Q-DLTS measurements allow direct determination of the time of carrier emission (relaxation of non-equilibrium charge) from the specified traps. These times are one of the switching process parameters. Emission (relaxation) time of non-equilibrium carriers is determined from the position of the corresponding peak maximum on the Q-DLTS spectrum. Table 1 shows the carrier emission time for all the detected traps measured at room temperature (300 K). It can be seen that among others there is E_3 center, for which the emission time is 10^{-6} s at 200 K. An increase in T leads to a shift of the Q-DLTS peak to a lower value of τ_m. The presence of ΔQ signal attributed to E_3 peak is observed at room temperature, but the Q-DLTS technique used is not able to evaluate the parameters of the recharging processes. Approximation of the temperature dependence of the emission time up to room temperature allowed for the estimation of the emission time as 700 ns at 300 K.

4. Discussion

Film from partially fluorinated graphene flakes consists of small graphene or few-layer graphene quantum dots. QD size can be estimated as several nanometers, and the thickness is 1–4 monolayers [9]. That very material was found to demonstrate the resistivity switching effect. Similar switching of the resistivity is observed for fluorinated graphene or few-layer CVD grown graphene with relatively large QDs (lateral size of ~70 nm) [12]. In the last case, stable resistivity switching is observed in the temperature range of 80–350 K at the same voltage with reproducible currents in high- and low-resistivity states at each temperature.

Generally, based on the transport and Q-DLTS data, we have revealed that the switching effect is bound with the reversible appearance of traps in the FG band gap under applied voltage. Let us consider these traps and start with the high-resistance state. The carrier emission from the main part of the traps in the high-resistance state is found to be the non-activated tunneling process between the unfluorinated areas of graphene flakes through the fluorinated barriers (see table 1). Different carrier emission times from traps E_{02}–E_{04} presumably correlate with the variation of potential barrier parameters (barrier height and/or thickness). The activation energy of traps E_{01} (0.50 eV) can be, most likely, interpreted as a potential barrier between the graphene and fluorinated graphene areas or between the FG film and valence bands of silicon substrate.

The following data are used for metal/FG/Si diagrams given in figure 6. The work function of Au is known to be equal to 5.3–5.5 eV [30]. The electron affinity for silicon is known to be equal to 4.05 eV, and for Si with a carrier concentration of ~5×10^{15} cm^{-3} the position of the Fermi level is estimated as ~0.2 eV from the valence or conductive band. The band gap of the FG depends on the fluorination degree. In the case of C-F the band gap is estimated as 3.0 eV [31]. In the case of C_4-F and one-sided saturated fluorination, the band gap of 2.93 eV was calculated [32]. Our films have composition between C_2-F and C-F, so, the band gap of 3.0 eV has been selected. The work function of fluorographene according to the theoretical studies [32, 33] is 6.0–7.3 eV. The work function of graphene is known to be equal to 4.3–4.6 eV [32, 34]. Experimental studies of charge transport in lateral graphene / FG / graphene transistor structures clearly demonstrate the presence of a potential barrier in such structures. The height of the latter potential barrier was estimated by Moon *et al* as 0.26 eV [35]. The temperature dependence of resistivity in few-layer graphene films with QDs, prepared by means of fluorination, also gives the potential barrier values 0.12 and 0.35 eV [24]. Based on the above given parameters, we have suggested that the work function of partially fluorinated graphene has a lower value in comparison

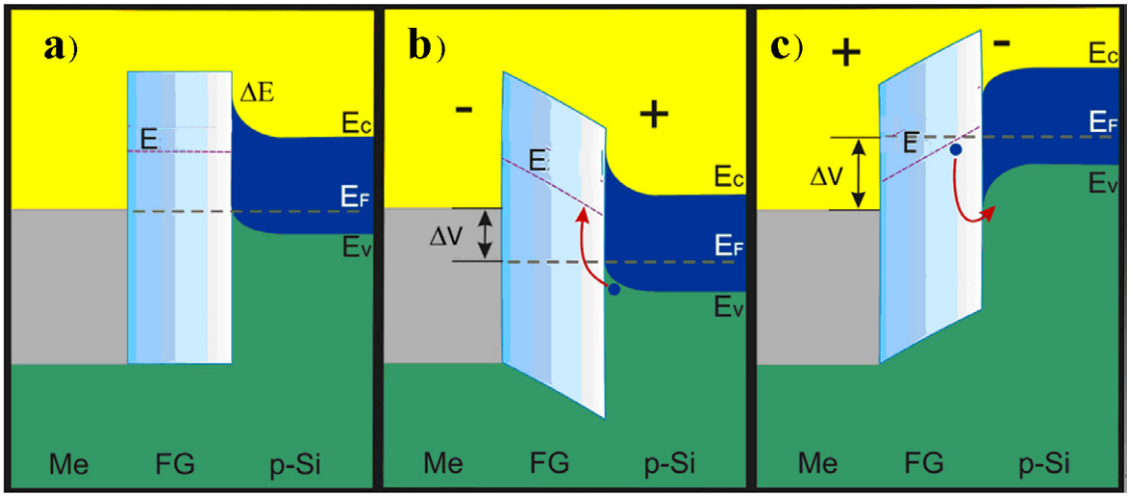

Figure 6. Expected band diagram of (a) Au / FG / p-Si structures at no voltage, (b) for the filling pulse $\Delta V = V_c + V_{fp}$, (c) during the carrier emission from the traps for holes at constant voltage, applied to the sample $\Delta V = V_c$. Only one trap is considered in this diagram, for simplicity. In order to observe the electron traps the positive polarity of voltage was applied to the film as the filling pulse, and the negative one was used for the carrier emission.

with fluorographene. As a result, for the case of C_2-F, the work function can be estimated as 5.2–5.5 eV (linear approximation), and the band offset ΔE with conductive band at the FG/Si interface in figure 6(a) will vary from 0.3 to 0 eV. It corresponds to the formation of an accumulated layer in p-type Si or a depleted layer in n-type Si (see figure 6(a)). Barriers between holes in graphene QDs and p-type Si substrates can be estimated as 0.34–0.64 eV. The activation energy for hole emission experimentally obtained for this case by *Q*-DLTS is equal to 0.50 eV. This value correlates to the given estimation. Within this interpretation, the barrier value for electrons in structures FG / p-Si will be higher (0.62 eV or more) and can be observed only at higher temperatures. So, as appears from the data given in table 1 only activationless carrier migration is going to occur in this case.

As mentioned above, from both the temperature dependences of current at the low temperatures and the data received by the *Q*-DLTS measurements at the high-conductivity mode (compare the traps in the high- and low-resistance states in table 1), it follows that the set of traps in the FG band gap is formed. The traps provide high conductivity, activated and fast non-activated carrier emission from localized states at low temperatures. The effect of resistance switching is usually associated with the formation of conductive channels in the material due to the migration of atoms or defects in the electric field (see, e.g. [36]). In the case of graphene oxide or SiO_2, the migration of oxygen atoms or metal atoms from the contacts is assumed [5, 14]. In our case, the formation of multiplied conductive channels is also suggested by means of trap introduction in a bandgap of fluorinated graphene. This partially fluorinated graphene considered in the present study consists of the graphene areas and the fluorographene network. The traps in the fluorinated part are provided by carrier transport in fluorinated graphene. The introduction of traps can be connected with the reorganization of fluorine atoms or defects. Partial fluorination of our material creates the conditions for small atom displacement or reconnection of fluorine bonds with adjacent carbon atoms for the appearance of the traps in the FG band gap, and the high concentration of introduced traps provides free migration of carriers in the film.

It follows from the data obtained by the *Q*-DLTS method, that several types of traps for electrons and holes with the density of 10^{10}–10^{12} cm^{-2} are formed in the FG film. The activation energies given in table 1 represent the difference between the energy of localized states in the FG band gap and the edge of the conduction band (electron traps) or the valence band (hole traps) of silicon. The substitution of p-type silicon for n-type silicon has enhanced our ability to monitor a wider spectrum of traps, which are responsible for the FG conducting state. Keep in mind that before the transition to the high-conductivity mode, the film resistance was 1–2 orders of magnitude higher, the density of localized states was ~10^{10} cm^{-2} or less, and only one type of activated process (passing of 0.5 eV potential barrier) was observed.

Trap E_3 with the activation energy of 0.08 eV (according to the *Q*-DLTS data) and the charge relaxation time of ~700 ns at room temperature attract particular attention. These very traps are also detected from the temperature dependences of current. Furthermore, trap E_3 has minimum values of the charge relaxation time, which makes it the most interesting trap in terms of the partially fluorinated graphene film application for the resistive memory. Relatively low concentrations of E_3 center according to the *Q*-DLTS measurements can be associated with the rapid emission of the carrier from these traps.

5. Conclusions

The films with a thickness of 50–100 nm, created from partially fluorinated graphene suspension, have been studied. As it turns out, these films demonstrate the resistive switching effect, which makes them promising for application as a material for the resistive memory. The traps in the layers of partially fluorinated graphene in the high-and the low-resistance state

were investigated using the charge spectroscopy technique. In the high-resistance state, only one type of activated process with energy of 0.5 eV has been found and may be interpreted as the overcoming of the potential barrier in structure GQDs/FG/Si. Other traps with zero activation energy also observed in the low-resistance state, most likely, correspond to carrier tunneling between graphene quantum dots through fluorinated graphene barriers with different parameters. The set of traps for electrons and holes in the band gap of fluorinated graphene was found in the films after their transition into the low-resistance state, and the trap energies and densities were defined. The times of carrier emission from different traps were determined, and it was demonstrated that the minimum time was ~700 ns for the traps with energy 0.08 eV. It is these traps that were found to determine carrier transport through the films. It is assumed that negligible fluorine displacement or just the fluorine bond reconnection to the neighboring carbon atoms can result in the conductive channel formation. The presence of these channels is also proved by the results of the carrier transport in the films.

Acknowledgments

The authors are grateful to W B Timofeev, Scientific Researcher of Ammosov North-Eastern Federal University, for his assistance in the scanning electron microscopy measurements. This study was financially supported in part by the Russian Foundation of Basic Research (Grant No. 15-02-02189). I I Kurkina was supported by the Russian Foundation of Basic Research (Grant No. 15-32-50088).

References

[1] Jeong D S, Thomas R, Katiyar R S, Scott J F, Kohlstedt H, Petraru A and Hwang S C 2012 *Rep. Prog. Phys.* **75** 076502
[2] Yang J J, Zhang M X, Strachan J P, Miao F, Pickett M D, Kelley R D, Medeiros-Ribeiro G and Williams R S 2010 *Appl. Phys. Lett.* **97** 232102
[3] Hermes C *et al* 2011 *IEEE Electron Device Lett.* **32** 1116–8
[4] Jeong H Y *et al* 2010 *Nano Lett.* **10** 4381–6
[5] Wang Z, Tjoa V, Wu L, Liu W J, Fang Z, Tran X A, Wei J, Zhu W G and Yu H Y 2012 *J. Electrochem. Soc.* **159** K177–82
[6] Yi M, Zhao L, Fan Q, Xia X, Ai W, Xie L, Liu X, Shi N, Wang W, Wang Y and Huang W 2011 *J. Appl. Phys.* **110** 063709
[7] Yin Z, Zeng Z, Liu J, He Q, Chen P and Zhang H 2013 *Small* **9** 727–31
[8] Midya A, Gogurla N and Ray S K 2015 *Curr. Appl. Phys.* **15** 706–10
[9] Kurkina I I, Nebogatikova N A, Antonova I V, Prinz V Ya, Aleksandrov G N, Timofeev V B, Smagulova S A, Zakirov E R and Kesler V G 2015 *Phys. Chem. Chem. Phys.* **17** 13257–66
[10] Dawlaty J M, Shivaraman S, Chandrashekhar M, Rana F and Spencer M G 2008 *Appl. Phys. Let.* **92** 042116
[11] Breusing M, Kuehn S, Winzer T, Malic E, Milde F, Severin N, Rabe J P, Ropers C, Knorr A and Elsaesser T 2011 *Phys. Rev.* B **83** 153410
[12] Antonova I V, Nebogatikova N A and Prinz V Ya 2014 *Appl. Phys. Lett.* **104** 193108
[13] Antonova I V, Nebogatikova N A, Prinz V Ya, Popov V I and Smagulova S A 2014 *J. Appl. Phys* **116** 134310
[14] Zhuge F, Fu B and Cao H 2013 *New Progress on Graphene Research* ed J R Gong (Rijeka: InTech) pp 185–206
[15] Yu A D, Liu C L and Chen W C 2012 *Chem. Commun.* **48** 383–5
[16] He C L, Shi Z W, Zhang L C, Yang W, Yang R, Shi D X and Zhang G Y 2012 *ACS Nano* **6** 4214–21
[17] Hu B L *et al* 2012 *J. Mater. Chem.* **22** 16422–30
[18] Nebogatikova N A, Antonova I V, Prinz V Ya, Volodin V A, Zatsepin D A, Kurmaev E Z, Zhidkov I S and Cholakh S O 2014 *Nanotechnol. Russ.* **9** 51–9
[19] Eda G and Chhowalla M 2010 *Adv. Mater.* **22** 2392–415
[20] Hernandez Y, Lotya M, Rickard D, Bergin S D and Coleman J N 2010 *Langmuir* **26** 3208–13
[21] Wang J, Hernandez Y, Lotya M, Coleman J N and Blau W 2009 *J Adv. Mater.* **21** 2430–5
[22] Zhao W, Wu F, Wu H and Chen G 2010 *J. Nanomater.* **2010** 528235
[23] Keeley G P, O'Neill A, Holzinger M, Cosnier S N, Coleman J N and Duesberg G S 2011 *Phys. Chem. Chem. Phys.* **13** 7747–50
[24] Nebogatikova N A, Antonova I V, Volodin V A and Prinz V Ya 2013 *Physica* E **52** 106–11
[25] Nebogatikova N A, Antonova I V, Prinz V Ya, Timofeev V B and Smagulova S A 2014 *Carbon* **77** 1095–103
[26] Lang D V 1974 *J. Appl. Phys.* **45** 3023–32
[27] Güttinger J, Molitor F, Stampfer C, Schnez S, Jacobsen A, Dröscher S, Ihn T and Ensslin K 2012 *Rep. Prog. Phys.* **75** 126502
[28] Malard L M, Pimenta M A, Dresselhaus G and Dresselhaus M S 2009 *Phys. Rep.* **473** 51–87
[29] Liu N, Luo F, Wu H, Liu Y, Zhang Ch and Chen J 2008 *J. Adv. Funct. Mater.* **18** 1518–25
[30] Skriver H L and Rosengaard N M 1992 *Phys. Rev.* B **46** 7157–68
[31] Nair R R *et al* 2010 *Small* **6** 2877–84
[32] Robinson J T *et al* 2010 *Nano Lett.* **10** 3001–5
[33] Giovannetti G, Khomyakov P A, Brocks G, Karpan V M, van den Brink J and Kelly P J 2008 *Phys. Rev. Lett.* **101** 026803
[34] Markevich A, Jones R and Briddon P R 2011 *Phys. Rev.* B **84** 115439
[35] Moon J S *et al* 2013 *IEEE Electron Device Let.* **34** 1190–2
[36] Tian H, Chen H-Y, Ren T-L, Li C, Xue Q-T, Mohammad M A, Wu C, Yang Y and Wong H-S P 2014 *Nano Lett.* **14** 3214–9